



1 **Estimating changes of temperatures and precipitation extremes in India using the**
2 **Generalized Extreme Value (GEV) distribution**
3

4 **Kishore Pangaluru^{1*}, Isabella Velicogna^{1,2}, Tyler C. Sutterley¹, Yara Mohajerani¹,**
5 **Enrico Ciraci¹, Jyothi Sompalli³, and Saranga Vijaya Bhaskara Rao³**
6

7 1. Department of Earth System Science, University of California, Irvine, California,
8 92697, USA

9 2. Jet Propulsion Laboratory, California Institute of Technology, Pasadena, California,
10 USA

11 3. Department of Physics, Sri Venkateswara University, Tirupati, India
12
13
14
15
16
17
18
19
20
21
22

23 ***Corresponding Author:**

24 **Email: kishore@uci.edu; Ph:1-949-824-3516**
25
26



27 **Abstract**

28 Changes in extreme temperature and precipitation may give some of the largest
29 significant societal and ecological impacts. For changes in the magnitude of extreme
30 temperature and precipitation over India, we used a statistical model of generalized
31 extreme value (GEV) distribution. The GEV statistical distribution is a time-dependent
32 distribution with different time scales of variability bounded by a precipitation, maximum
33 (T_{\max}), and minimum (T_{\min}) temperature extremes and also assessed their possibility
34 changes are evaluated and quantified over India is presented. The GEV-based method is
35 applied on both precipitation and temperature extremes over India during the 20th and 21st
36 centuries using multiple coupled climate models taking an interest in the Coupled Model
37 Intercomparison Project Phase 5 (CMIP5) and observational datasets. The regional means
38 of historical warm extreme temperatures are 34.89, 36.42, and 38.14 °C for three different
39 (10, 20, and 50-year) periods, respectively; whereas the cold extreme mean temperatures
40 are 7.75, 4.19, and -1.57 °C. It indicates that 20th century cold extreme temperatures have
41 relatively larger variations than the warm extremes. As for the future, the CMIP5 models
42 of warm extreme regional mean values increase from 0.33 to 0.75 °C in all return periods
43 (10-, 20-, and 50-year periods), while in the case of cold extreme means values vary
44 between 0.58 and 2.29 °C. In the future, cold extreme values have a larger increasing rate
45 over the northwest, northeast, some parts of north central, and Inter Peninsula regions.
46 The CRU precipitation extremes are larger than the historical extreme precipitation in all
47 three (10, 20, and 50-year) return-periods.

48

49 Keywords: Precipitation, surface temperature, GEV, Historical, and CMIP5.



50 **1. Introduction**

51 Extreme weather events, amplified by climate change, can lead to major
52 environmental issues affecting human society. Precipitation and temperature are two
53 major components of a changing climate that have been analyzed extensively over the
54 past two decades (Trenberth and Shea 2005; Li et al., 2009; Kharin et al., 2013).
55 According to the United Nations Office for Disaster Risk Reduction UNISDR (2015),
56 India is the third most influenced nation by weather related by disasters, which can
57 largely be attributed to both higher occurrences of extreme temperatures and precipitation.
58 Recently, Trenberth (2005) showed that climate change due to increased greenhouse gas
59 emissions leads to changes in extreme event behavior in terms of precipitation and
60 temperature all over the world. Generalized Extreme Value (GEV) statistical distribution
61 has long been used to examine time-series of climate extremes with different return levels
62 using three extreme value distributions that were proposed by Fisher and Tippet (1928).
63 The three distributions are referred to as Gumbel, Frechet, and negative Weibull, which
64 are discussed in Section 2. Jaruskova and Rencova (2008) studied the extreme changes in
65 annual maxima and minima temperature series using five meteorological sites,
66 implementing extreme value theory and hypothesis testing within the framework of the
67 GEV-based method.

68 Jenkinson (1955) used GEV distribution for extreme precipitation events, which
69 offered extensive adaptability of the three extreme value distributions. Later, several
70 researchers used GEV statistical distribution to study extreme precipitation for many
71 regions and different countries around the world (Fowler and Kilsby 2003; Nadarajah
72 2005; and Gilleland and Katz 2006). In China, a warming trend has been confirmed in



73 both annual minimum and maximum temperature in the twentieth century (Choi et al.
74 2009; You et al. 2011). Later studies also showed notable extreme temperature increases
75 in northeastern China, and the smallest increase in the southern region (Liu et al. 2004).
76 The frequency of extreme temperature events in China is expected to increase at an
77 accelerating rate based on Coupled Model Inter-comparison Project (CMIP) historical
78 projections (Wang and Chen 2014; Yang et al. 2014). Utilization of GEV distribution on
79 temperature and precipitation over China has been extensively studied in several
80 investigations (Wang and Zhou 2005; Zhang et al. 2011; Yang et al. 2014). As for India,
81 Shashikanth et al. (2017) applied a GEV distribution to GCM summer monsoon
82 precipitation in India during 1961-1990 and 2081-2100. They found a slight increase in
83 the future extreme spatial mean in the later period. However, the statistical GEV
84 distributions of extreme minimum and maximum temperatures in India have not been
85 examined in any previous studies. We utilize this method over India to address this issue.
86 CMIP models and observations are discussed in Section 2. The GEV statistical
87 distribution methodology is described in Section 3. Section 4 presents the results of the
88 GEV distribution in three different periods and occurrences over India, and finally the
89 conclusions are discussed in Section 5.

90 **2. Data and Method**

91 The observational dataset of gridded monthly precipitation (P), minimum and
92 maximum surface temperatures (T_{\min} and T_{\max}) are taken from the study of the Climate
93 Research Unit (CRU TS3.1) described by Harris et al. (2014). The datasets are collected
94 from 1901 to 2005 over land areas, based on daily values from rain gauge measurements
95 provided by more than 4,000 weather stations distributed around the world (New et al.,



96 1999, 2000). The precipitation and surface temperatures are collected from different
97 sources, with rigorous quality checking procedures before gridding (Mitchell and Jones,
98 2005; Harish et al., 2014). Figure 1 shows the Indian map with seven regions.

99 The monthly precipitation, and the minimum and maximum surface temperatures
100 (T_{\min} and T_{\max}) are simulated by CMIP5 (Coupled Intercomparison Project Phase 5)
101 models for a historical (hereafter referred to as "Historical") period from 1850 to 2005
102 (Smith et al., 2013; Lamarque et al., 2010) as well as the 21st century (years 2006-2100)
103 employing four different representative concentration pathways (RCPs) (Moss et al.,
104 2010, Taylor et al., 2012). The Historical and different scenarios of CMIP5 models are
105 listed in Table 1. Further details on the models and their configuration are described in
106 the references, online at <http://www-pcmdi.llnl.gov/>. We have considered only models for
107 which the same ensemble member i.e. 'r1i1p1' is available both in the historical and four
108 (RCP2.6, RCP4.5, RCP6.0, and RCP8.5) scenarios considered here. According to the
109 IPCC Fifth Assessment Report, the CMIP5 models exhibit improvements in the
110 simulations especially surface temperature and precipitation compared to the previous
111 climate models (Flato et al. 2013). The outputs for both historic and different RCPs
112 outputs are available on different spatial scales, which are consequently regridded to a
113 common spatial scale of 1° in latitude and 1° in longitude resolution.

114 Out of the monthly CMIP5 model outputs (listed in Table 1), Historical
115 experiments, RCP (2.6, 4.5, 6.0, and 8.5) experiments of T_{\min} , T_{\max} , and Precipitation (P)
116 are utilized for our analysis.



117 Three types of extreme distributions compose a GEV distribution: Gumbel,
118 Frèchet, and Weibull, also known as type I, II, and III respectively (Martins and
119 Stedinger 2000; Feng et al., 2007). These can generally be described by

$$120 \quad G((z; \mu, \sigma, \xi) = \begin{cases} \exp\left\{-\exp\left[-\left(\frac{z-\mu}{\sigma}\right)\right]\right\}, & \xi = 0 \\ \exp\left\{-\left[1 + \xi \frac{z-\mu}{\sigma}\right]^{-\xi^{-1}}\right\}, & \xi \neq 0, 1 + \xi \frac{z-\mu}{\sigma} > 0 \end{cases} \quad (1)$$

121 where μ , σ and ξ are the location, scale, and shape parameters, respectively.
122 Particular cases of Eq. (1) with $\xi \rightarrow 0$, $\xi > 0$, and $\xi < 0$ correspond to the Gumbel,
123 Frèchet, and the negative Weibull distributions, respectively. Generally, the value of ξ is
124 greater than zero for precipitation data, although the distribution of Gumbel is sometimes
125 adequate.

126 Several methods have been developed for the estimation of the parameters of
127 GEV distributions. These include the method of moments by Christopheit (1994), the less
128 influenced method of L-moments (Hosking, 1990; Hosking and Wallis, 1997); the
129 Bayesian method by Smith and Naylor (1987), Coles and Tawn (2005). The most popular
130 method is the maximum likelihood method (Smith and Naylor, 1987; Unkašerić and
131 Tošić, 2009), which has the advantage of allowing the addition of fitting co-variables
132 (such as trends, cycles or physical variables) (Katz et al., 2002). The detailed procedure
133 of these methods summarized by the El Adlouni et al. (2007), Kioutsioukis et al. (2010),
134 and Kharin et al. (2013). In this study, the maximum likelihood method is used to
135 estimate the parameters of the GEV distribution. The regression parameters of
136 $\mu(t)$, $\sigma(t)$, and $\xi(t)$ are the location, scale, and shape respectively. The parameters of the
137 likelihood function, given n observations $\{(t_1, z_1), (t_2, z_2), \dots, (t_n, z_n)\}$ at period t_i at which
138 the greatest z_i is acquired, is provided by



$$139 \quad L(\theta|t_t, z_t) = \prod_{i=1}^m g[z_i; \mu(t_i), \sigma(t_i), \xi(t_i)] \quad (2)$$

140 where

$$141 \quad g(z; \mu, \sigma, \xi) = \frac{1}{\sigma} \left\{ \left[1 + \xi \left(\frac{z-\mu}{\sigma} \right) \right]^{-(1+1/\xi)} \right\} \exp \left\{ - \left[1 + \xi \left(\frac{z-\mu}{\sigma} \right) \right]^{-1/\xi} \right\} \quad (3)$$

142 The log-likelihood function is

$$143 \quad l(\theta|t_t, z_t) = -\sum_{i=1}^m \left\{ \log \sigma(t_i) + \left(1 + \frac{1}{\xi(t_i)} \right) \log \left[1 + \xi(t_i) \left(\frac{z_i - \mu(t_i)}{\sigma(t_i)} \right) \right] + \left[1 + \right. \right. \\ 144 \quad \left. \left. \xi(t_i) \left(\frac{z_i - \mu(t_i)}{\sigma(t_i)} \right) \right]^{-\frac{1}{\xi(t_i)}} \right\} \quad (4)$$

145 $\sigma(t_i) > 0$ and $\{1 + \xi(t_i)(z_i - \mu(t_i))/\sigma(t_i) > 0\}$ for $i=1, \dots, n$. For every value of $\xi(t_i)$

146 that equals to zero, it is important to utilize the suitable limiting form, replacing the GEV

147 by the Gumbel (Eq. (1) for $\xi = 0$) log-likelihood function,

$$148 \quad l(\theta|t_j, z_j) = -\log \sigma(t_j) - \frac{z_j - \mu(t_j)}{\sigma(t_j)} - \exp \left[-\frac{z_j - \mu(t_j)}{\sigma(t_j)} \right] \quad (5)$$

149 The maximum likelihood estimate of θ yields the maximization of Eq. (4) and/or Eq. (5).

150 Rao (1973) estimated the confidence intervals for the selected return periods using the

151 delta method. Figure 1 shows the regression, model fits and estimated the return values of

152 monthly maximum temperatures.

153 We implement this GEV analysis to study the minimum and maximum surface

154 temperatures and precipitation as simulated by CMIP5 models in the historical

155 experiments (years 1901-2005), CRU observations, and experiments for the 21st century

156 (years 2006-2100) with four different radiative forcing scenarios.

157 **3. Results**

158 **3.1 CMIP Historical and CRU temperature extremes**



159 The spatial distribution of extremes for the Historical runs in India during 1901-
160 2005 is presented by showing maximum and minimum temperature extremes with
161 different return time periods are shown in Figure 2. The top and bottom panels show
162 maximum and minimum extremes respectively with return periods of 10, 20 and 50 years,
163 denoted as $T_{(\max,10)}$, $T_{(\max,20)}$, and $T_{(\max,50)}$ for maximum temperatures and $T_{(\min,10)}$, $T_{(\min,20)}$,
164 $T_{(\min,50)}$, for minimum temperatures respectively. The regional mean value for each return
165 time period is mentioned at the top of each plot. The mean values indicate high warm
166 extreme temperature conditions in India with average values of 34.89, 36.42, and 38.14°C
167 for $T_{(\max,10)}$, $T_{(\max,20)}$, and $T_{(\max,50)}$ respectively. The mean CRU extreme regional values
168 are 34.80, 36.46, and 38.42°C for the 10, 20, and 50 year periods (Figure not shown).
169 $T_{(\max,10)}$ and $T_{(\max,20)}$ show the most evident warm extremes over Northwest and North-
170 central regions. These extreme regions extend to the Interior peninsula at $T_{(\max,50)}$. Similar
171 extreme warm surface temperatures are observed over the northwestern part of India
172 (Gadgil, 2018). These three regions show maximum extremes with return values all
173 above 40°C, while the Western Himalaya region exhibits the lowest maximum
174 temperature extremes at about 10°C. At $T_{(\max,10)}$ large cold extremes cover most parts of
175 the Western Himalaya region and slowly turn to warming extremes at $T_{(\max,50)}$. The
176 minimum temperature extremes show large variations over India except for the Western
177 Himalaya region. The mean value of minimum temperature extreme over the entire
178 region in India is 7.75, 4.19, and -1.57°C for three (10, 20 and 50-year) return periods,
179 respectively. More extreme cold changes are observed in Figure 2 over the northeastern
180 and western regions of India, and cold temperature extremes drop from 7°C to -20°C for



181 10 and 50 years period. The warmer and colder extremes of the minimum temperature are
182 observed over southern and northern parts of India respectively.

183 **3.2 CMIP Historical and CRU changes in temperature extremes**

184 The spatial differences between CMIP and CRU warm and cold temperature
185 extremes for the three return estimates of 10, 20, and 50 year periods are shown in Figure
186 3. The upper and lower panels display the changes in warm and cold temperature
187 extremes for three time periods respectively. The positive (red color) and negative (blue
188 color) values in these diagrams indicate the warmest and coldest Historical extremes for
189 the three different periods.

190 The difference between the warm extremes decreases slightly from the 10 to 50-
191 year period over central and northern parts of India. Warm and cold bands are clearly
192 observed over the southern regions of the warm extreme difference map. Looking at the
193 cold extreme differences, a cold band (with a magnitude of $\sim 4.5^{\circ}\text{C}$) is observed in the
194 northwest region of India for the 50-year period, indicating that the CRU cold extremes
195 are warmer than those of CMIP5 historical runs. The regional mean value decreases from
196 0.14 to -0.20°C for warm extremes and decreases from -0.55 to -0.95°C for cold extremes
197 from 10 to 50 year periods. From Figure 3, the magnitude of the difference of cold
198 extremes is little larger than those of the warm extremes for all three return periods over
199 India. The mean value of warm and cold extreme differences are less than a degree
200 indicating a fairly good agreement between the Historical and CRU temperatures for the
201 three different return periods. Kharin et al. (2005, 2007) observed that the temperature
202 differences between CMIP5 multi-model and ERA-Interim are generally larger for cold
203 extremes than for warm extremes during the period from 1986 to 2005. Table 2



204 summarizes the warm and cold extreme temperature mean values for the 10, 20, and 50-
205 year periods of each region for the CRU, Historical, as well as the differences between
206 the two. It is evident from the table that the maximum warm extreme mean temperature is
207 observed in the Interior Peninsula over the Historical ensemble and CRU temperatures
208 for the 20- and 50-year return periods.

209 **3.4 Future climate extreme changes in CMIP5 projections**

210 The spatial GEV distribution for three different return values of 10, 20, and 50
211 years estimated from CMIP5 maximum temperatures of different RCP scenarios (RCP
212 2.6, 4.5, 6.0, and 8.5) for the period 2006-2099 are shown in Figure 4. All RCPs suggests
213 comparable spatial distributions of maximum temperatures over the three different
214 periods. The spatial distributions of warm extremes for all RCPs look similar in the 50-
215 year period. Moderately warm regional mean temperature changes are observed in
216 RCP2.6 and RCP8.5 scenarios at about 1.15, 1.28, and 1.28°C for the three (10, 20 and 50
217 year) periods, respectively. In RCP2.6, the warm temperature extremes are observed in
218 northwest (NW) and north central (NC) regions in the 10-year period, while warm
219 extremes cover three regions (NW, NC, and IP) in the 20-year period, and most of the
220 regions in India in the 50 year period. In RCP8.5 the maximum temperatures are
221 observed in most of the Indian regions with regional means of 39.96, 39.99, and 41.18°C
222 for the three (10, 20, and 50-year) return periods, respectively. Maximum extreme
223 temperatures of about ~44°C are observed in several grids throughout India under (RCP
224 2.6 and 8.5) CMIP5 experiments in the 20 and 50 year return periods. Similar extreme
225 temperatures reach values of around 46°C in large areas of northwest and Interior
226 peninsula regions over equatorward of 25°. All simulations demonstrate an ascent of



227 more than $\sim 3.5^{\circ}\text{C}$ over three regions (NW, NC, and IP), and a warming of more than 2°C
228 over the western Himalayan region in the 50 year period.

229 The spatial distribution of cold temperature extremes during the 21st century
230 under the RCP scenarios (RCP 2.6, 4.5, 6.0, and 8.5) for the three different time periods
231 over India are shown in Figure 5. The regional mean values of cold extremes have
232 consistently decreasing trends in all RCP scenarios. The northwest, western Himalayas,
233 and northeast are the main regions exhibiting diminishing trends in all three return
234 periods. The mean value of cold extremes for the 50-year period is $\sim 7^{\circ}\text{C}$ higher than the
235 20-year period for RCP2.6. For the other concentration pathways (RCP 4.5, 6.0 and 8.5),
236 the projected increase in cold temperature extremes ranges from 2.5°C to 2.8°C , and 3.3°
237 C to 3.9°C over the period 10 to 20 and 20 to 50-year return periods, respectively. Note
238 that the positive changes of about $\sim 5^{\circ}\text{C}$ in temperature are observed in the RCP8.5
239 experiment in 21st century relative to the 1901-1960 historic period (Basha et al., 2017).
240 The cold temperature extreme slowly decreases with latitude from south to north of India
241 in all RCP scenarios. The magnitude at the southern tip of India is about 20°C , which
242 decreases to -23°C over the northern tip. The maximum regional cold extreme value at
243 about 12.73°C is observed in RCP8.5 for a 10-year period, while the minimum at about -
244 0.99°C is observed in RCP2.6 for 50-year return period.

245 **3.5 Temperature extremes inter-model uncertainty in CMIP5 projections:**

246 The variability of the warm and cold temperature extremes over India can be
247 shown by standard deviations as shown in Figures 6 and 7, which depict the spatial
248 distributions of standard deviations for three different time periods (10, 20, and 50-year)
249 of warm (T_{\max}) and cold (T_{\min}) extremes projected in the four different scenarios (RCP2.6,



250 4.5, 6.0, and 8.5), respectively. The spatial map in Figure 6 indicates the maximum to be
251 in the southern part of Interior Peninsula (IP), while the second maximum (relatively
252 weak) is at the Western Himalaya (WH) region in RCP2.6 at the 50-year period. The
253 standard deviation of warm extremes is larger in the 50-year period compared to the 10-
254 and 20-year periods especially in the southern part of India in all RCP scenarios. The
255 maximum mean value is about 0.75°C in RCP8.5 (10-year period), whereas the minimum
256 value is observed in RCP2.6 (50-year return value) at about 0.33°C . The standard
257 deviations change in small increments across different scenarios for all return periods.
258 For example, the standard deviation changes in 20-year return values are 0.47, 0.45, 0.41,
259 0.49°C under RCP2.6, 4.5, 6.0, and 8.5 scenarios, respectively.

260 The spatial distribution of different CMIP5 experiments for three different time
261 periods (10, 20, and 50-year) return values of cold extreme (T_{\min}) standard deviations are
262 shown in Figure 7. A distinct feature of warm bias (up to 3.5°C) in eastern and western
263 regions of India is observed in all scenarios at 20- and 50-year periods. In cold extremes,
264 the 50-year return period standard deviation is higher compared to other return values
265 under RCP2.6. The maximum mean value of $T_{\min,50}$ is about 2.29°C in RCP2.6, while the
266 minimum value ($T_{\min,10}$) is observed in RCP8.5. The cold extremes have a larger
267 variability comparing to warm temperature extremes. The mean maximum value of warm
268 temperatures ($T_{\max,50}$) is almost three times as large as the $T_{\min,50}$ in RCP2.6. The
269 variability of warm extremes (given by the standard deviation) are spatially fairly
270 uniform in all the return periods, which is not the case for cold extremes under CMIP5
271 scenarios. Recent observational (Lee et al., 2014) and modeling (Kharin et al., 2007,
272 2013) studies have reported larger variability of warming in cold extremes compared to



273 warm extremes across different return periods. This indicates that variability in cold
274 temperature extremes is larger than those of warm temperature extremes over India.

275 **4. Precipitation extremes**

276 **4.1 Historical and CRU precipitation extremes and differences**

277 The spatial variations of Historical (top panel), CRU (middle panel), and the
278 differences between the two (bottom panel) of extreme precipitation for three different
279 return periods (10, 20, and 50-year) are shown in Figure 8. The three (10, 20, and 50-
280 year) periods of precipitation extremes are computed from the GEV procedure by using
281 monthly precipitation grids. From Figure 8, precipitation extremes increase significantly
282 from the 10 to the 50-year period in both Historical and CRU observations. In
283 CMIP5_historical runs the extreme precipitation appears to have a positive trend in the
284 Interior Peninsula, which extends slightly into North Central (NC) part of India. The
285 maximum trends, however is concentrated in the IP region. In the case of CRU, the
286 increasing trend is observed over the IP and NC regions for the 20-year period, which
287 also extends to most parts of India except for the southern tip and the Western Himalayan
288 regions for the 50-year period. A widespread increase in extreme precipitation is
289 observed in CRU for the 50-year period over the IP, NC, WC and EC regions. The
290 differences between Historical and CRU extreme precipitations indicate that the CRU
291 extreme values are slightly higher over the IP and NC, while Historical is slightly higher
292 in the northern and southern parts of India for the 10- and 20-year periods. In the 50-year
293 period, precipitation is higher in the Historical runs compared to CRU over the Interior
294 Peninsula, Western Himalayan regions. However, extreme precipitation is lower in the
295 Historical runs, in the northwest and extending to northwest and extending to north-



296 central regions of India. The regional mean differences are -11.89%, -11.33% and 4.69%
297 for all three (10, 20, and 50-year) periods, respectively.

298 The multi-model extreme precipitation differences for the 10-, 20-, and 50-year
299 return periods during the period 2006-2100 for each CMIP5 scenarios (RCP2.6, 4.5, 6.0,
300 and 8.5) relative to the 1901-2005 historical periods are shown in Figure 9. The
301 northwestern region has the greatest decrease in all CMIP5 scenarios for all three return
302 periods, which implies that the warmest region has the greatest decrease in extreme
303 precipitation in future projections. The maximum mean difference is about ~23% in
304 RCP8.5 for the 50-year return period. In comparison, future projections of extreme
305 precipitation are slightly higher than Historical ones in the northern and some regions
306 within Interior Peninsula. However, the Historical precipitation extremes are dominant in
307 the 50-year period, and to a smaller extent in the 10-year period. The regional mean
308 changes of extreme precipitation for the 50-year period are -10.4%, -12.9%, -4.3%, and -
309 22.9% under the RCP2.6, 4.5, 6.0, and 8.5 scenarios, respectively. From Figure 9, the
310 regional mean changes of future precipitation extremes are 1.9% and 5.9% in RCP2.6
311 (20-year period) and RCP6.0 (20-year period), respectively. Shashikanth et al. 2017 also
312 found that significant changes in monsoon precipitation extremes during a 30-year period
313 (2081-2100) compared to the historic period.

314 **5. Conclusions**

315 We have assessed the Historical and CRU precipitation and temperature extremes
316 and likely future changes within them throughout India. We quantified the warm and cold
317 temperatures as well as precipitation extremes of CMIP5 for all Representative
318 Concentration Pathway scenarios (RCP2.6, 4.5, 6.0, and 8.5) for the future using a



319 statistical model of climate extremes based on GEV distributions for the three return
320 periods (10, 20, and 50-year). The most important findings of our analysis are
321 summarized as follows:

322 Extreme warm values in Historical T_{\max} in India appear to be rather moderate.
323 The regional means of extreme maximum temperatures are 34.89, 36.42, and 38.14 °C for
324 all three (10, 20, and 50-year) return periods, respectively, while the minimum extreme
325 temperatures are 7.75, 4.19, -1.47 °C for those same return periods. Comparing the 10- to
326 50-year return periods, the warm extremes increase at about ~3 °C over northwestern,
327 north central, and Interior peninsula regions. Cold extremes are decreased ~5 °C
328 especially over the eastern and western regions of India.

329 The regional relative mean differences of Historical and CRU T_{\max} extremes are
330 0.14, 0.01 and -0.20 °C for the three (10, 20, and 50-year) periods, respectively.
331 Comparing the 10- and 50-year return periods shown that the relative changes of extreme
332 temperatures decrease in Northwest, North central, and northern part of Interior peninsula,
333 and increase over lower part of the west coast. The relative mean differences of CRU
334 cold extremes are slightly higher than those of the Historical runs. The relative mean
335 differences of cold extremes are -0.55, -0.64, and 0.28 °C for the three (10, 20, and 50-
336 year) periods, respectively. CRU shows more changes in the cold extremes as opposed to
337 warm extremes compared to the Historical extremes. Regionally, northwestern and
338 northeastern regions of India show the highest changes.

339 Future T_{\max} extreme temperatures increase in all RCP scenarios compared to
340 historical temperatures, especially for the 20 and 50 year periods. The regional extreme
341 mean values increase moderately compared to the historical values at about 1.85 and 2.92



342 °C in the 50-year period under RCP6.0 and 8.5 scenarios. In the case of T_{\min} extreme
343 mean temperatures of RCP2.6 decrease by nearly 5 °C compared to the historical values,
344 while the minimum extreme temperature mean in RCP8.5 increase by nearly 4 °C
345 compared to historical temperatures in 50-year return period. It must be noted that the
346 effect of increasing radiative forcing under higher concentration pathways is larger on
347 cold temperatures compared to warm temperatures.

348 The spatial variability of CRU extreme precipitation rates is substantially larger
349 compared to Historical extremes in all three return periods. Upon comparing 10-, and 50-
350 year periods, changes in precipitation extremes are observed in both the location and
351 scale of the distribution, especially over North Central and Interior Peninsula regions of
352 India. In the other regions, CRU precipitation extreme changes increase slightly in the
353 50-year period. The regional mean relative difference of Historical and CRU precipitation
354 extremes is observed the 50-year period at about -14.6%. It indicates that Historical
355 precipitation extremes show smaller values compared to CRU in several regions in India.
356 The past and future differences of extreme precipitation are significantly larger when
357 comparing to Historical to RCP8.5, implying that increasing radiative forcing under
358 higher greenhouse gas concentrations may lead to larger changes in precipitation
359 extremes.

360 **Acknowledgements**

361 We acknowledge the GCM modeling groups, the Program for Climate Model
362 Diagnosis and Inter-comparison (PCMDI), and the WCRP's Working Group on Coupled
363 Modeling for their roles in making available WCRP CMIP5 multi-model datasets. The



364 authors would like to thank the National Center for Atmospheric Research (NCAR) for
365 providing the CRU data.

366 **Figure captions**

367 Figure 1. Sample plot of Generalized Extreme Value (GEV) distribution return values,
368 empirical and modeled fits with 95% confidence level, together with the map of
369 India divided in the seven regions used in this study.

370 Figure 2. The historical maximum temperature (T_{\max} ; top panel), and minimum
371 temperature (T_{\min} ; bottom panel) extremes for 10-year (left), 20-year (middle),
372 and 50-year (right) periods during 1901-2005.

373 Figure 3. The difference between CMIP5_historical and CRU maximum temperature
374 (T_{\max} ; top panel), and minimum temperature (T_{\min} ; bottom panel) extremes for
375 (left) 10-year, (right), 20-year, and (right) 50-year periods during 1901-2005.

376 Figure 4. The (left) 10-year, (middle) 20-year, and (right) 50-year return values of CMIP5
377 multi-model mean of warm temperature extremes for the period 2006-2100
378 under RCP2.6 (1st row), RCP4.5 (2nd row), RCP6.0 (3rd row), and RCP8.5
379 (bottom row) scenarios, together with the regional average stated on top of each
380 panel.

381 Figure 5. The (left) 10-year, (right) 20-year, and (right) 50-year return values of CMIP5
382 multi-model minimum temperature extremes projected in 2006-2100 under
383 RCP2.6 (1st row), RCP4.5 (2nd row), RCP6.0 (3rd row), and RCP8.5 (bottom
384 row) experiments, together with the regional means stated on top of each panel.

385 Figure 6. The CMIP5 inter-model standard deviations for the 10-year (left), 20-year
386 (middle), and 50-year (right) return values of warm temperature extremes



387 simulated in the RCP2.6 (1st row), RCP4.5 (2nd row), RCP6.0 (3rd row), and
388 RCP8.5 (bottom row) experiments, respectively.

389 Figure 7. The CMIP5 inter-model standard deviations for the 10-year (left), 20-year
390 (middle), and 50-year (right) return values of cold temperature extremes
391 simulated in the RCP2.6 (1st row), RCP4.5 (2nd row), RCP6.0 (3rd row), and
392 RCP8.5 (bottom row) experiments, respectively.

393 Figure 8. The 10-year (left), 20-year (middle), and 50-year (right) return values of
394 Historical (1st row), CRU (2nd row), and the relative change between Historical
395 and CRU (%), bottom row) of precipitation extremes during 1901-2005.

396 Figure 9. The CMIP5 multi-model mean relative change (%) for the 10-year (left), 20-
397 year (middle), and 50-year (right) return values of precipitation extremes
398 between the historic values in 1901-2005 and the simulated values in 2006-2100
399 under RCP2.6 (1st row), RCP4.5 (2nd row), RCP6.0 (3rd row), and RCP8.5
400 (bottom row) scenarios, together with their regional means of relative changes
401 on top of each panel.

402

403

404

405

406

407

408

409



410 **References:**

- 411 Choi, G., Collins, D., Ren, G. Y. et al.: Changes in means and extreme events of
412 temperature and precipitation in the Asia-Pacific network region, 1955-2007. *Int.*
413 *J. Climatol.*, 29, 1906-1925, 2009.
- 414 Fisher R. A., and Tippett, L. H. C.: Limiting forms of the frequency distribution of the of
415 a sample, *Proce. Cambridge Philos. Soc.*, 180-190, 1928
- 416 Flato, G., Marotzke, J., Abiodun, B., Braconnot, P., Chou, S. C., Collins, W., Cox, P.,
417 Driouech, F., Emori, S., Eyring, V., Forest, C., Gleckler, P., Guilyardi, E., Jakob,
418 C., Kattsov, V., Reason, C., Rummukainen, M.: Evaluation of climate models. In:
419 Stocker TF et al (eds) *Climate Change 2013: the physical science basis*,
420 Cambridge University Press, Cambridge, 741-866, 2013.
- 421 Flower, H. J., and Kilsby, C. G.: A regional frequency analysis of United Kingdom
422 extreme rainfall from 1961 to 2000, *International Journal of Climatology*, 23(11),
423 1313-1334. doi: 10.1002/(ISSN)1097-0088, 2003.
- 424 Gadgil, S.: The monsoon system: Land-sea breeze or the ITCZ?. *J. Earth Syst. Sci.*, 5,
425 127. doi:10.1007/s12040-017-0916-x, 2018.
- 426 Gilleland, E., Katz, R.: Analyzing seasonal to interannual extreme weather and climate
427 variability with the extremes toolkit. In 18th Conference on Climate Variability
428 and Change, 86th American Meteorological Society (AMS) Annual Meeting, 20
429 January – 2 February, 2006, Atlanta, Georgia, 2006.
- 430 Harrish, I., Jones, P., Osborn, T., and Lister, D.: Updated high resolution grids of
431 monthly climate observations-The CRU TS3.10 dataset, *Int. J. Climatol.*, 34, 623-
432 642. doi: 10.1002/joc.3711, 2014.
- 433 Jaruskova, D., and Rencova, M.: Analysis of annual maximum and minimal temperatures
434 for some European cities by change point methods, *Environmetrics*, 19(3), 221-
435 233. doi: /10.1002/env.865, 2008.
- 436 Jenkinson, A. F.: The frequency distribution of the annual maximum (or minimum)
437 values of meteorological elements, *Quart. J. Roy. Meteor. Soc.*, 81, 158-171, 1955.
- 438 Kharin, V. V., Zwiers, F. W., Zhang, X., and Hegerl, G. C.: Changes in temperature and
439 precipitation extremes in the IPCC ensemble of global coupled model simulations,
440 *J. Climatol.*, 20, 1419-1444, 2007.



- 441 Kharin, V. V., and Zwiers, F. W.: Estimating extremes in transient climate change
442 simulations, *J. Climatol.*, 18, 1156-1173, 2005.
- 443 Kharin, V. V., Zwiers, F. W., Zhang, X., and Wehner, M.: Changes in temperature and
444 precipitation extremes in the CMIP5 ensemble, *Climate Change*, 119, 345-357,
445 2013.
- 446 Lamarque, J. -F., Bond, T. C., Eyring, V., Granier, C., Heil, A., Klimont, Z., Lee, D.,
447 Liousse, C., Mieville, A., Owen, B., Schultz, M. G., Shindell, D., Smith, S. J.,
448 Stehfest, E., Van Aardenne, J., Cooper, O. R., Kainuma, M., Mahowald, N.,
449 McConnell, J. R., Naik, V., Riahi, K., and Van Vuuren, D. P.: Historical (1850-
450 2000) gridded anthropogenic and biomass burning emissions of reactive gases and
451 aerosols: Methodology and application, *Atmos. Chem. Phys.*, 10, 7017-7039.
452 doi:10.5194/acp-10-7017-2010, 2010.
- 453 Li, L., Hong, Y., Wang, J. H., Adler, R. F., Policicelli, F. S., Habib, S., Irwn, D., Korme,
454 T., Okello, L.: Evaluation of the real-time TRMM-based multi-satellite
455 precipitation analysis for an operational flood prediction system in Nzoia basin,
456 lake Victoria, Africa, *Natural Hazards*, 50, 109-123, 2009.
- 457 Liu, B. H., Xu, M., Henderson, M., et al.: Taking China's temperature: daily range,
458 warming trends, and regional variations, *J. Climatol.*, 17, 4453-4462, 2004.
- 459 Mitchell, T. D., and Jones, P. D.: An improved method of constructing a database of
460 monthly climate observations and associated high-resolution grids, *Int. J.*
461 *Climatol.*, 25, 693-712, 2005.
- 462 Moss, R. H., Edmonds, J. A., Hibbard, K. A., Manning, M. R., Rose, S. K., Van Vuuren,
463 D. P., Carter, T. R., Emori, S., Kainuma, M., Kram, T., Meehl, G. A., Mitchell, J.
464 F. B., Nakicenovic, N., Riahi, K., Smith, S. J., Stouffer, R. J., Thomson, A. M.,
465 Weyant, J. P., and Wilbanks, T. J.: The next generation of scenarios for climate
466 change research and assessment, *Nature*, 463, 747-756. doi:10.1038/nature08823,
467 2010.
- 468 Nadarajah, S.: Extremes of daily rainfall in west central Florida, *Climate Change*, 69,
469 325-342, 2005.



- 470 New, M., Hulme, M., and Jones, P.: Representing twentieth century space-time climate
471 variability. Part 1: development of a 1961-90 mean monthly terrestrial climatology,
472 J. Climate, 12, 829-856, 1999.
- 473 New, M., Hulme, M., Jones, P. D.: Representing twentieth century space-time climate
474 variability, II: development of 1901-1996 monthly grids of terrestrial surface
475 climate, J. Climate, 13, 2217-2238, 2000.
- 476 Pickandas, J.: Statistical Inference Using Extreme Order Statistics, The Annals of
477 Statistics, 3, 119-131, 1975.
- 478 Shashikanth, K., Ghosh, S., Vittal, H., and Karmakar, S.: Future projections of Indian
479 summer monsoon rainfall extremes over India with statistical downscaling and its
480 consistency with observed characteristics, Clim. Dyn., doi: 10.1007/s00382-017-
481 3604-2, 2017.
- 482 Smith, T. M., Arkin, P. A., Sapiano, M. R. P.: Merged statistical analyses of historical
483 monthly precipitation anomalies beginning 1990, J. Climatol., 23, 5755-5770,
484 2010.
- 485 Taylor, K. E., Stouffer, R. J., and Meehl, G. A.: An overview of CMIP5 and the
486 experiment design. Bull. Am. Meteorol. Soc., 93, 485-498. doi:10.1175/BAMS-
487 D-11-00094.1, 2012.
- 488 Trenberth, K.E.: Uncertainty in hurricanes and global warming, Science, 308, 1753-1754,
489 2005.
- 490 Trenberth, K.E., and Shea, D. J.: Relationships between Precipitation and Surface
491 temperature, Geophys. Res. Lett., 32, L14703, doi: 10.1029/2005GL022760, 2005.
- 492 Wang, L., Chen, W.: A CMIP5 multi model projection of future temperature,
493 precipitation, and climatological drought in China, Int. J. Climatol., 34, 2059-
494 2078, 2014.
- 495 Wang, Y. Q., and Zhou, L.: Observed trends in extreme precipitation events in China
496 during 1961-2001 and the associated changes in large-scale circulation. Geophys.
497 Res. Lett., 32, 4, 2005.
- 498 Yang, S. L., Feng, J. M., Dong, W. J., and Chou, J.: Analysis of extreme climate events
499 over China based on CMIP5 historical and future simulations, Adv. Atmos. Sci.,
500 31, 1209-1220, 2014.



501 You, Q. L., Kang, S. C., Aguilar, E., et al.: Changes in daily climate extremes in China
502 and their connection to the large scale atmospheric circulation during 1961-2003,
503 Clim. Dyn., 36, 2399-2417, 2011.

504 Zhang, L., Dong, M., and Wu, T. W.: Changes in precipitation extremes over Eastern
505 China simulated by the Beijing Climate Center Climate System Model
506 (BCC_CSM1.0), Clim. Res., 50, 227-245, 2011.

507
508
509
510
511
512
513
514
515
516
517
518
519
520
521
522
523
524
525
526
527
528
529
530
531
532
533
534
535
536
537
538
539
540
541
542
543



544
 545
 546
 547
 548
 549
 550
 551
 552
 553
 554
 555
 556
 557
 558
 559
 560
 561
 562
 563
 564
 565
 566
 567
 568
 569
 570
 571
 572
 573
 574
 575
 576
 577
 578
 579
 580
 581
 582
 583
 584
 585
 586
 587
 588
 589

Table 1: Historical and CMIP5 different scenarios (RCP2.6, RCP4.5, RCP6.0, and RCP8.5) precipitation and maximum and minimum temperature

Model Name	Historical 1901-2005		CMIP5 2006-2099							
	Stem	Pr	Stem				Pr			
			RCP2.6	RCP4.5	RCP6.0	RCP8.5	RCP2.6	RCP4.5	RCP6.0	RCP8.5
CCSM4	Y	Y	Y	Y	Y	Y	Y	Y	Y	Y
CNRM-CM5	Y	Y	Y	Y	Y	Y	Y	Y	Y	Y
CSIRO-MK3	Y	Y	Y	Y	Y	Y	Y	Y	Y	Y
CanESM2	Y	Y	Y	Y	Y	Y	Y	Y	Y	Y
GFDL-CM3	Y	Y	Y	Y	Y	Y	Y	Y	Y	Y
GISS-E2-H	Y	Y	Y	Y	Y	Y	Y	Y	Y	Y
GISS-E2-R	Y	Y	Y	Y	Y	Y	Y	Y	Y	Y
HadGEM2-CC	Y	Y	Y	Y	Y	Y	Y	Y	Y	Y
HadGEM2-ES	Y	Y	Y	Y	Y	Y	Y	Y	Y	Y
IPSL-CM5A-LR	Y	Y	Y	Y	Y	Y	Y	Y	Y	Y
MIROC-ESM	Y	Y	Y	Y	Y	Y	Y	Y	Y	Y
MIROC5	Y	Y	Y	Y	Y	Y	Y	Y	Y	Y
MPI-ESM-LR	Y	Y	Y	Y	Y	Y	Y	Y	Y	Y
MRI-CGCM3	Y	Y	Y	Y	Y	Y	Y	Y	Y	Y
NorESM1-M	Y	Y	Y	Y	Y	Y	Y	Y	Y	Y
BCC-CSM1-1	Y	Y	Y	Y	Y	Y	Y	Y	Y	Y
INMCM4	Y	Y	Y	Y	Y	Y	Y	Y	Y	Y
GFDL-ESM2M	N	N	N	N	N	N	N	N	N	N
BNU-ESM	N	N	N	N	N	N	N	N	N	N
IPSL-CM5A-MR	N	N	N	N	N	N	N	N	N	N
CANESM2	Y	Y	Y	Y	Y	Y	Y	Y	Y	Y
FGOALS-g2	Y	Y	Y	Y	Y	Y	Y	Y	Y	Y
CESM1-CAM5	Y	Y	Y	Y	Y	Y	Y	Y	Y	Y



590
591
592
593
594
595
596
597
598

Table 2: CRU and differences between CRU and historical maximum and minimum temperature and standard deviation for seven homogeneous regions for 10-, 20-, and 50-year return periods.

Regions	CRU: T _{max}			CRU: T _{min}			CMP - CRU: T _{max}			CMP - CRU: T _{min}		
	Avg ± std			Avg ± std			Avg ± std			Avg ± std		
	10 year	20 year	30 year	10 year	20 year	30 year	10 year	20 year	30 year	10 year	20 year	30 year
India	34.80 ± 5.87	36.46 ± 6.15	38.42 ± 6.83	9.77 ± 8.07	6.51 ± 8.39	1.86 ± 10.04	0.14 ± 1.19	0.01 ± 1.05	-0.20 ± 1.46	-0.55 ± 0.82	-0.64 ± 0.31	-0.95 ± 2.12
IP	37.51 ± 1.59	40.12 ± 2.19	43.92 ± 3.33	15.55 ± 1.92	13.72 ± 2.53	11.51 ± 3.48	0.27 ± 1.06	0.09 ± 1.33	-0.30 ± 2.08	-0.35 ± 0.29	-0.75 ± 0.61	-1.52 ± 1.42
EC	35.62 ± 1.41	36.78 ± 1.63	38.08 ± 2.07	17.48 ± 2.90	15.17 ± 3.37	11.67 ± 6.42	-0.29 ± 2.03	-0.17 ± 1.96	0.01 ± 0.83	0.31 ± 0.49	0.31 ± 0.49	0.61 ± 0.95
NC	37.91 ± 2.82	39.81 ± 3.03	41.91 ± 3.44	9.76 ± 2.67	5.76 ± 3.42	0.19 ± 5.32	1.33 ± 1.51	0.77 ± 1.36	-0.13 ± 1.43	-0.28 ± 0.45	0.03 ± 1.03	0.57 ± 1.57
NW	38.13 ± 4.26	39.37 ± 4.33	40.47 ± 4.42	8.16 ± 3.06	3.98 ± 1.72	-1.54 ± 1.88	1.14 ± 0.56	0.85 ± 0.53	0.49 ± 0.51	-0.89 ± 0.69	-1.32 ± 0.76	-2.75 ± 3.86
WC	34.59 ± 2.27	35.83 ± 2.59	37.41 ± 3.18	16.44 ± 2.77	14.43 ± 3.03	11.63 ± 5.03	-0.33 ± 0.93	0.21 ± 1.22	1.37 ± 1.57	-0.01 ± 0.58	-0.64 ± 0.26	-2.28 ± 2.09
NE	30.46 ± 5.48	31.44 ± 5.65	32.31 ± 5.86	6.69 ± 5.78	1.10 ± 4.45	-8.99 ± 6.68	-1.33 ± 1.96	-1.42 ± 2.01	-1.54 ± 2.03	-0.93 ± 0.96	-0.69 ± 1.38	-0.11 ± 2.03
WH	18.14 ± 5.52	19.59 ± 5.36	20.74 ± 5.23	-13.75 ± 7.14	-15.71 ± 8.39	-17.53 ± 7.32	-2.28 ± 1.52	-1.63 ± 1.15	-0.89 ± 1.76	-2.02 ± 0.68	-1.87 ± 0.68	-1.67 ± 0.68

IP = Interior Peninsula; EC = East Coast; NC = North Central; NW = North West; WC = West Coast; NE = North East; WH = Western Himalayas.

599
600
601
602
603
604
605
606
607
608
609
610
611
612
613
614
615
616



617
 618
 619
 620
 621
 622
 623
 624
 625
 626
 627
 628
 629
 630
 631
 632
 633
 634
 635
 636
 637
 638
 639
 640
 641
 642
 643
 644
 645
 646
 647
 648
 649
 650
 651
 652
 653
 654
 655
 656
 657
 658
 659
 660
 661
 662

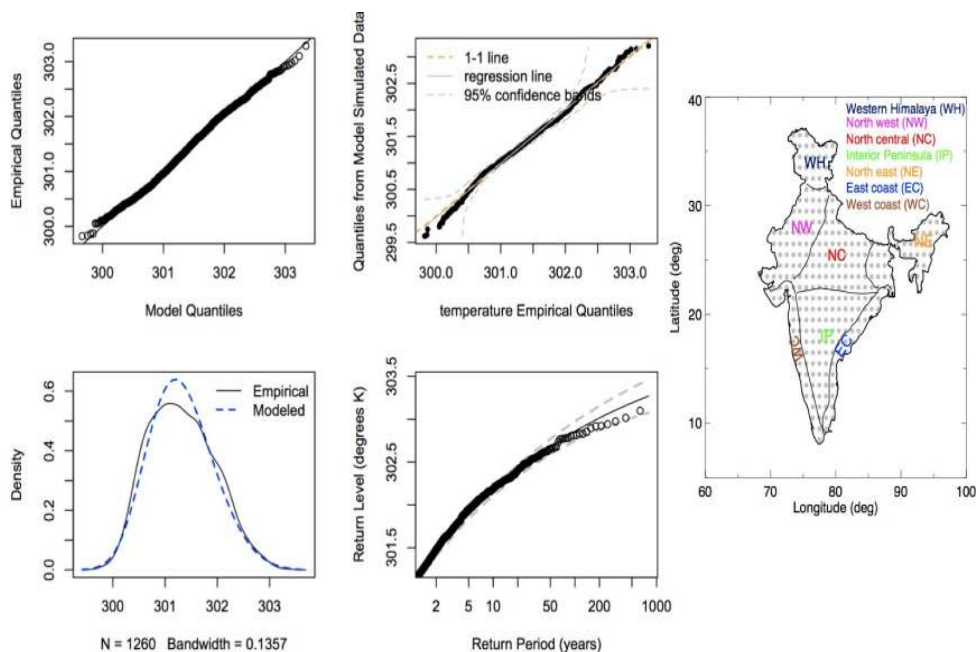


Figure 1



663
664
665
666
667
668
669
670
671
672
673
674
675
676
677
678
679
680
681
682
683
684
685
686
687
688
689
690
691
692
693
694
695
696
697
698
699
700
701
702
703
704
705
706
707
708

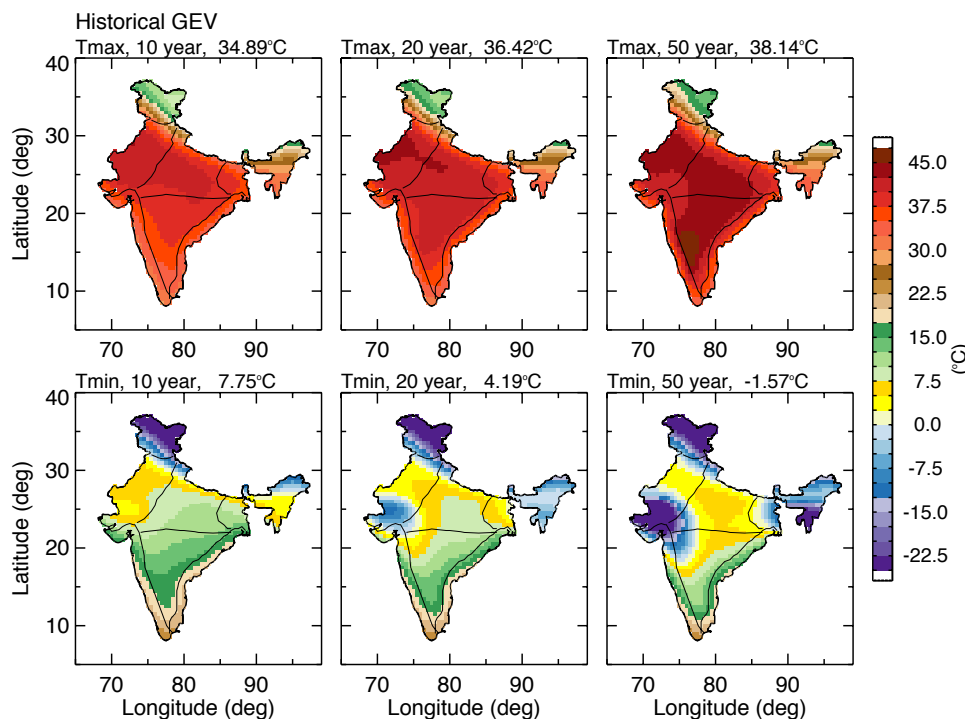


Figure 2



709
710
711
712
713
714
715
716
717
718
719
720
721
722
723
724
725
726
727
728
729
730
731
732
733
734
735
736
737
738
739
740
741
742
743
744
745
746
747
748
749
750
751
752
753
754

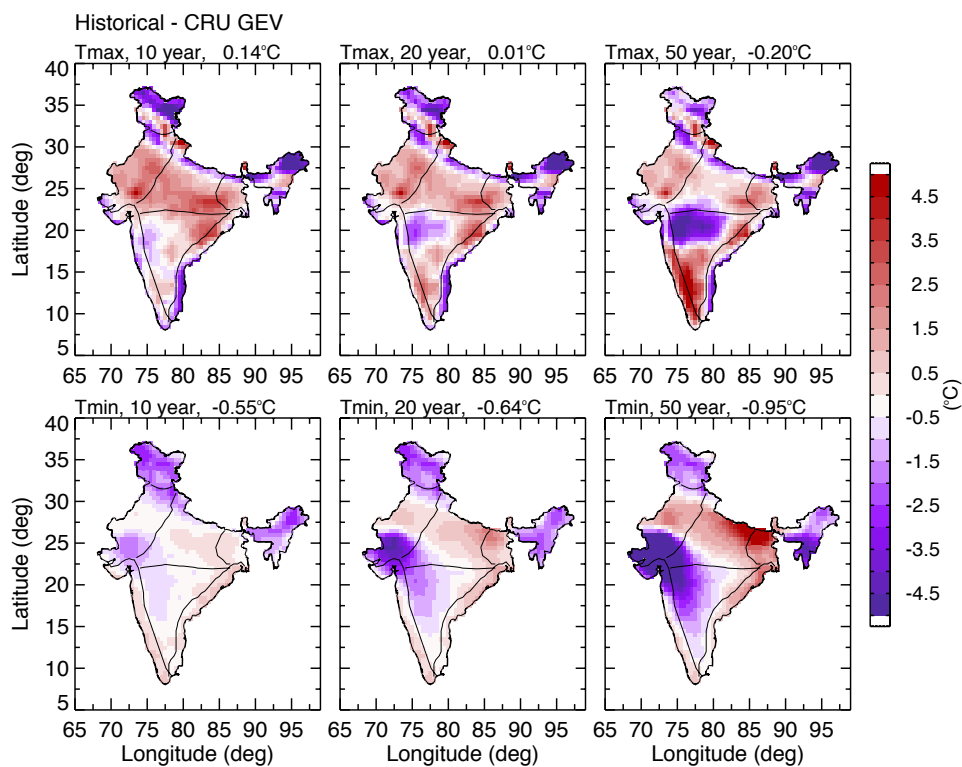


Figure 3



755
756
757
758
759
760
761
762
763
764
765
766
767
768
769
770
771
772
773
774
775
776
777
778
779
780
781
782
783
784
785
786
787
788
789
790
791
792
793
794
795
796
797
798
799
800

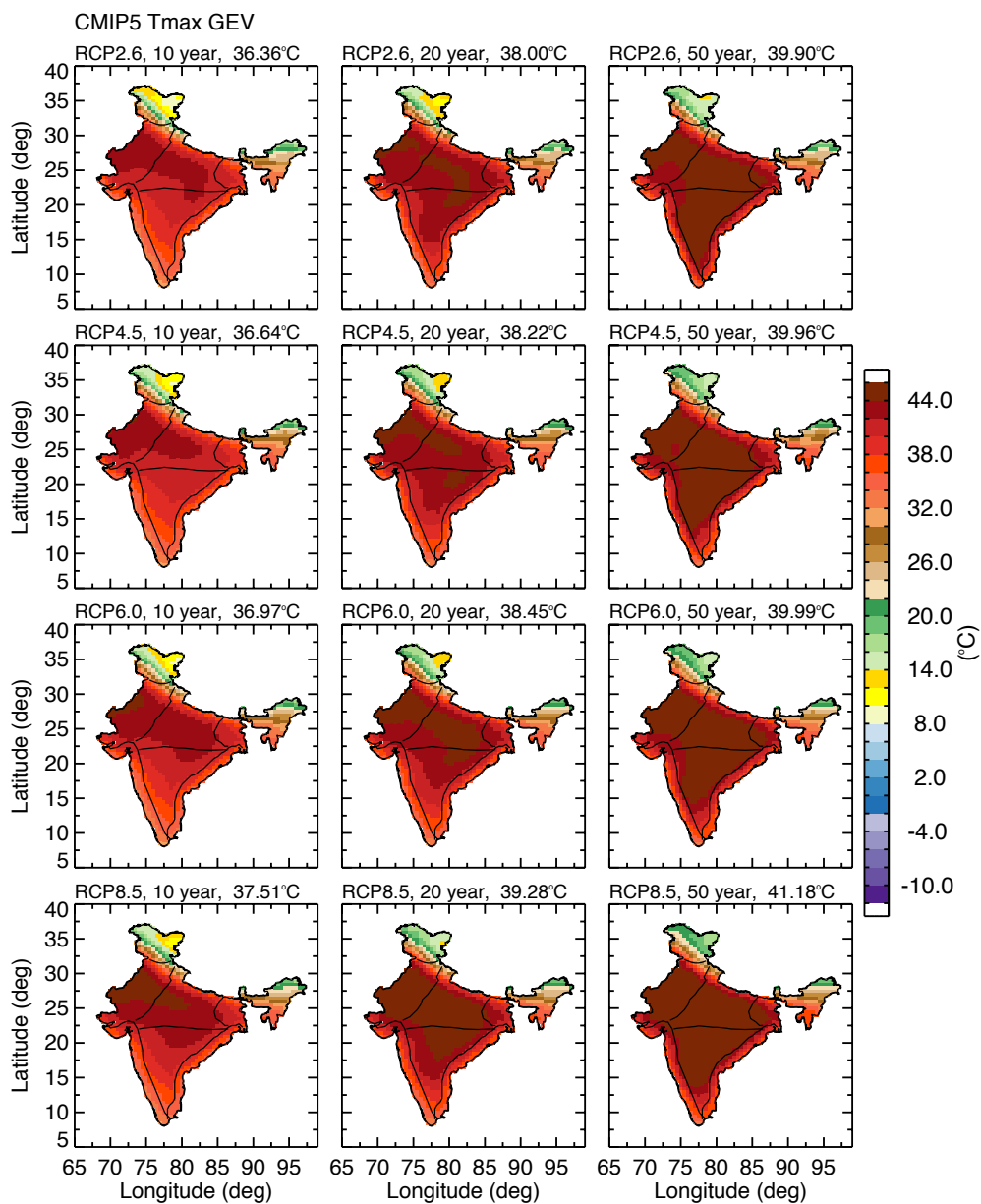


Figure 4



801
802
803
804
805
806
807
808
809
810
811
812
813
814
815
816
817
818
819
820
821
822
823
824
825
826
827
828
829
830
831
832
833
834
835
836
837
838
839
840
841
842
843
844
845
846

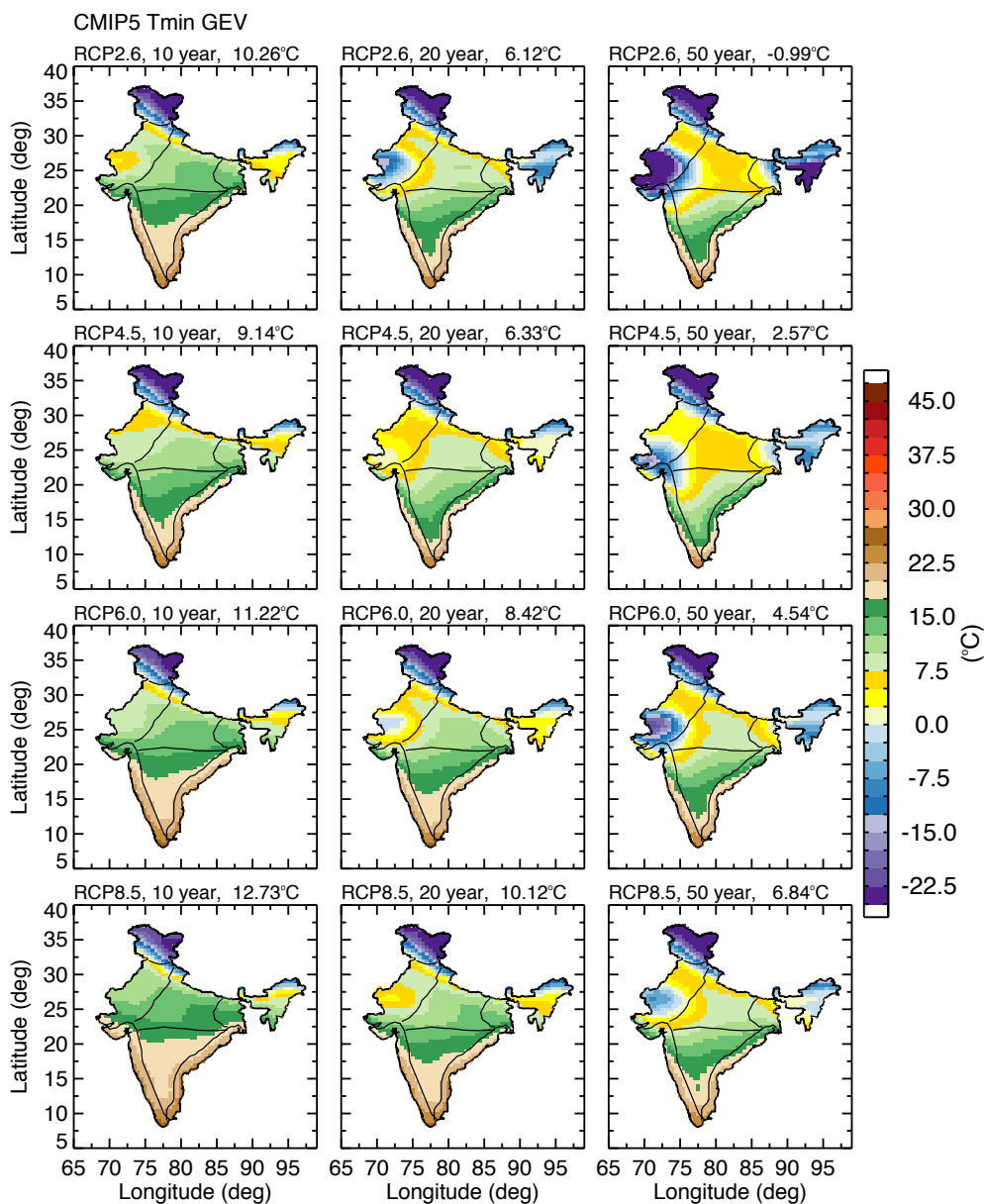


Figure 5



847
 848
 849
 850
 851
 852
 853
 854
 855
 856
 857
 858
 859
 860
 861
 862
 863
 864
 865
 866
 867
 868
 869
 870
 871
 872
 873
 874
 875
 876
 877
 878
 879
 880
 881
 882
 883
 884
 885
 886
 887
 888
 889
 890
 891
 892

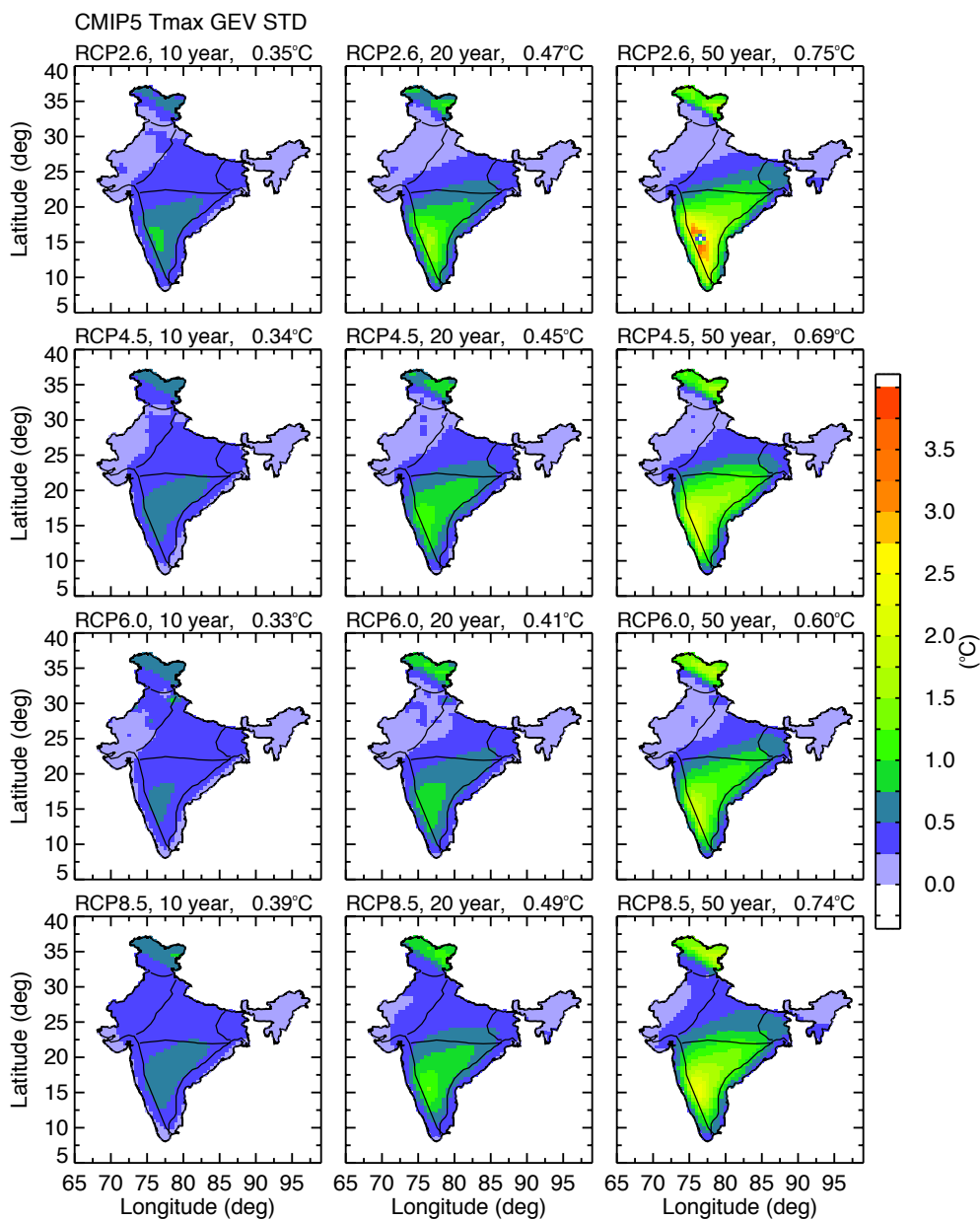


Figure 6



893
 894
 895
 896
 897
 898
 899
 900
 901
 902
 903
 904
 905
 906
 907
 908
 909
 910
 911
 912
 913
 914
 915
 916
 917
 918
 919
 920
 921
 922
 923
 924
 925
 926
 927
 928
 929
 930
 931
 932
 933
 934
 935
 936
 937
 938

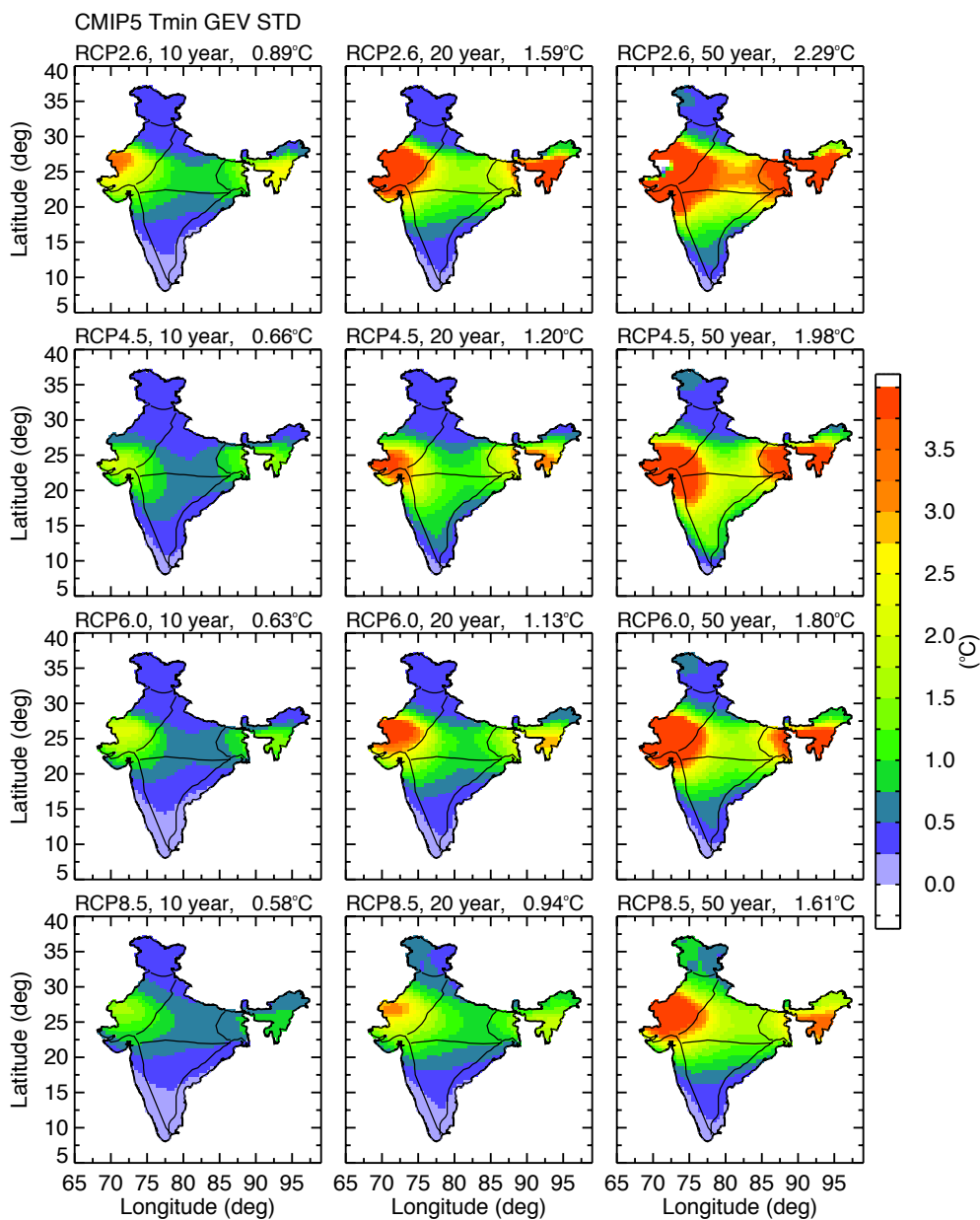


Figure 7



939
940
941
942
943
944
945
946
947
948
949
950
951
952
953
954
955
956
957
958
959
960
961
962
963
964
965
966
967
968
969
970
971
972
973
974
975
976
977
978
979
980
981
982
983
984

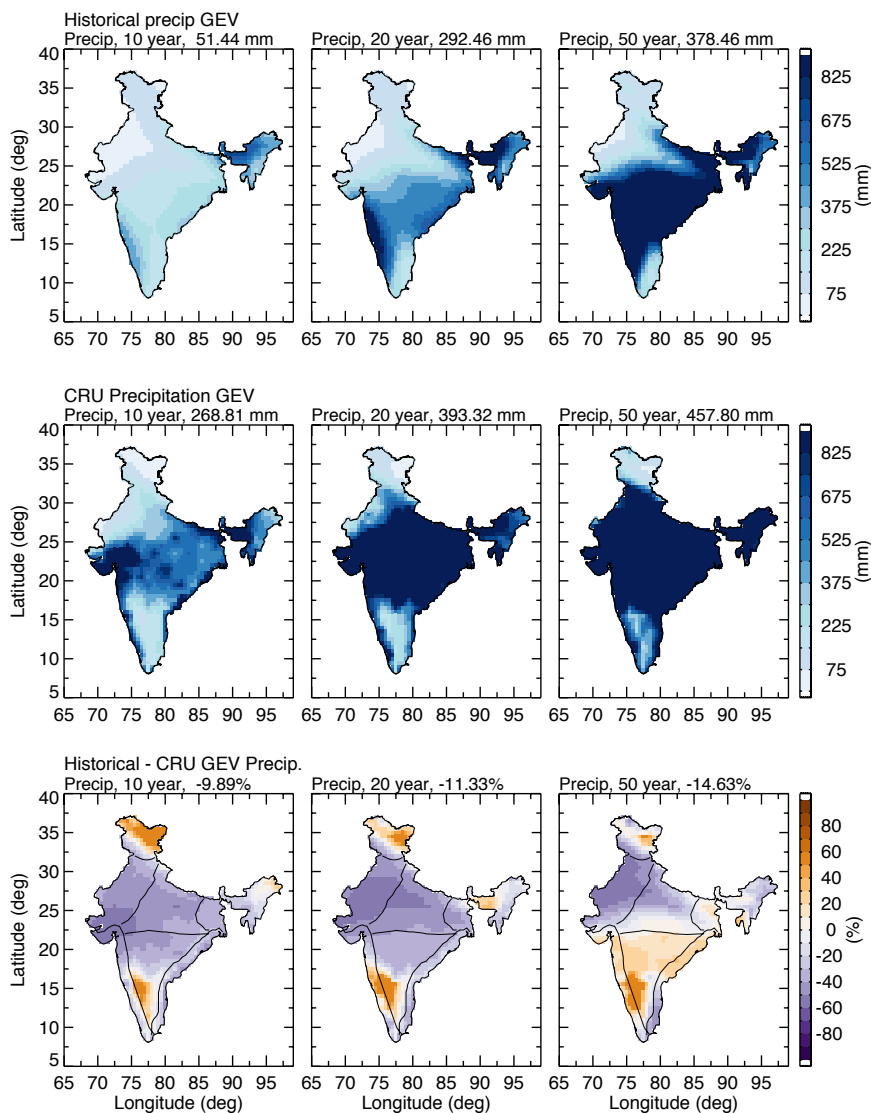


Figure 8



985
 986
 987
 988
 989
 990
 991
 992
 993
 994
 995
 996
 997
 998
 999
 1000
 1001
 1002
 1003
 1004
 1005
 1006
 1007
 1008
 1009
 1010
 1011
 1012
 1013
 1014
 1015
 1016
 1017
 1018
 1019
 1020
 1021
 1022
 1023
 1024
 1025
 1026
 1027
 1028
 1029
 1030

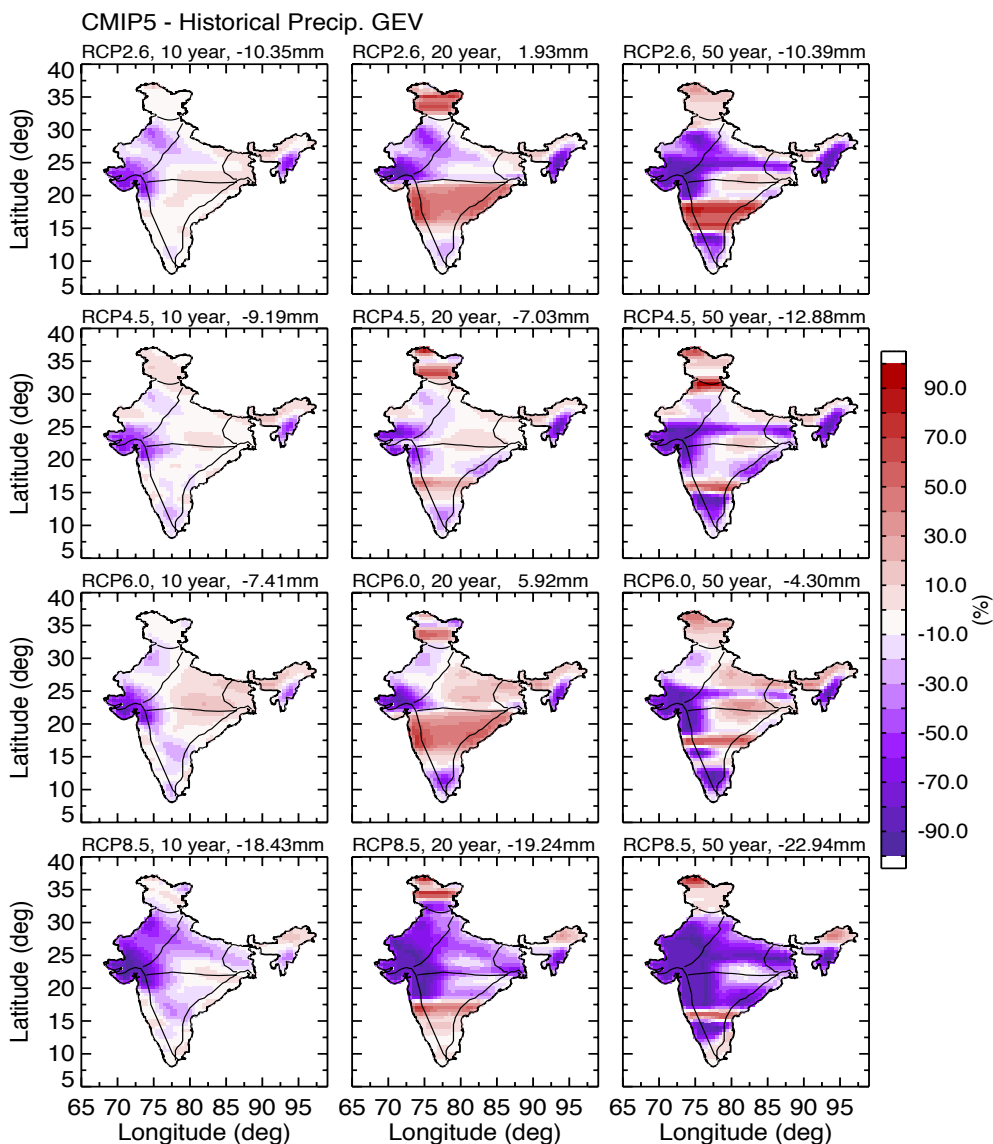


Figure 9